Journal Pre-proof

Experimental and Quantum Investigations of Novel Corrosion
Inhibitors based Triazene Derivatives for Mild Steel

M.H. Mahross , Mahmoud A. Taher , M.A. Mostfa ,
Kwok Feng Chong , Gomaa A.M. Ali
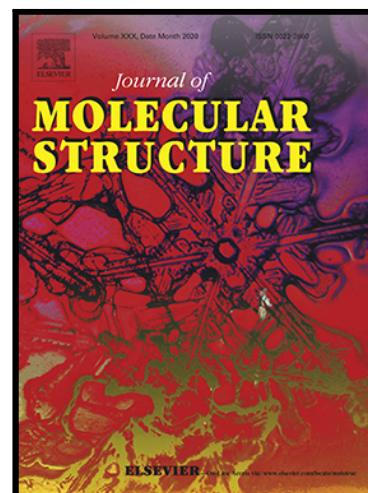
Please cite this article as: M.H. Mahross , Mahmoud A. Taher , M.A. Mostfa , Kwok Feng Chong ,
Gomaa A.M. Ali , Experimental and Quantum Investigations of Novel Corrosion Inhibitors
based Triazene Derivatives for Mild Steel, *Journal of Molecular Structure* (2021), doi:
https://doi.org/10.1016/j.molstruc.2021.130831

Highlights

- Triazene derivatives were used as novel corrosion inhibitors

- Different electrochemical techniques were used to study the inhibition behavior

- Triazene compounds showed a high inhibition activity of 98.51%

- Quantum chemical calculations supported the electrochemical findings

Experimental and Quantum Investigations of Novel Corrosion Inhibitors based Triazene Derivatives for Mild Steel

M. H. Mahross [a,*], Mahmoud A. Taher [a], M. A. Mostfa [a], Kwok Feng Chong [b], Gomaa A.M. Ali [a,*]

[a] Chemistry Department, Faculty of Science, Al–Azhar University, Assiut 71524, Egypt

[b] Faculty of Industrial Sciences & Technology, Universiti Malaysia Pahang, Gambang, 26300 Kuantan, Malaysia

* Corresponding author: mahmoud_mahross@yahoo.com (M.H. Mahross), gomaasanad@azhar.edu.eg (G.A.M. Ali)

2

Graphical Abstract
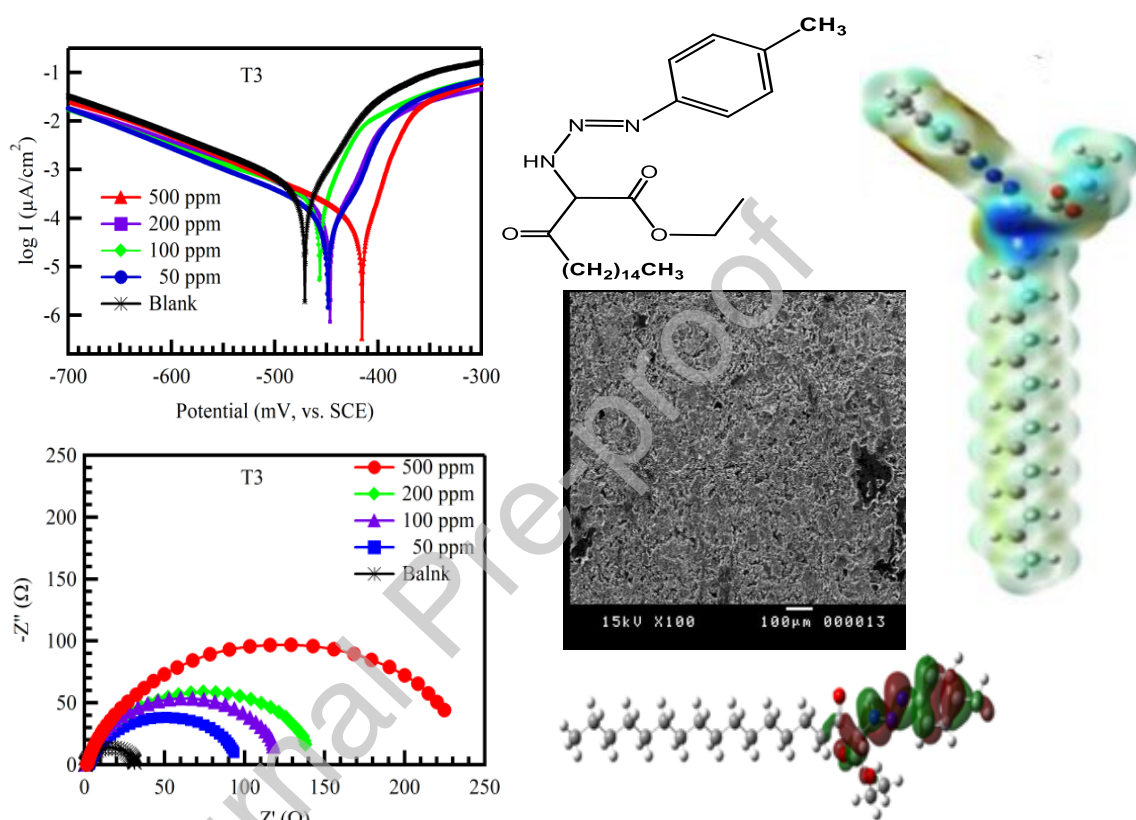
Abstract

The present work investigates some triazene compound's anti-corrosion properties as novel corrosive inhibitors by experimental and theoretical studies. Different electrochemical and morphological techniques were used to study the compound's corrosion inhibition. The experiments were performed in 1 M H_2SO_4 at different inhibitor concentrations and temperatures. The results showed that triazene compounds are effective inhibitors for mild steel corrosion in an acidic medium. Gaussian 09W software was used to calculate the compound's quantum chemical data, and there was an excellent approval between the experimental and quantum chemical calculations.

Keywords: Corrosion Protection, Mild Steel, Acidic, Triazene Derivatives, Quantum computation.

1. Introduction

Mild steel (MS) is a metal used in different industrial fields, and it is susceptible to corrosion because of exposure to different corrosive environments. Sulfuric acid is widely used in industrial processes, but it negatively affects the metal surface due to SO_4^{2-} ions that act as an aggressive ion effect on the surface of metals [1]. Industrial operating processes at high temperatures are most vulnerable to the significant loss of their metal components to corrosion. In acidic media, metals corrosion rate gradually increases by increasing temperature [2, 3]. Inhibitors are substances added to a corrosive medium by low concentration to protect the metal from acid attack [4, 5]. Organic substances with heterocyclic atoms (N, O, S, and P) are excellent inhibitors [6-9]. Their inhibition action depends on the molecular parameters such as lone pair of electrons, steric factors, planarity, and energy gap [10]. These heterocyclic compounds can be adsorbed on the metallic surface, and they behave as both physical and chemical inhibitors [11, 12]. Pyridine-based Schiff bases and triazole derivatives inhibited MS corrosion in acidic medium and exhibited a high efficiency of 98.58% [10] and 95.50% [12], respectively. Triazenes are organic compounds in their structures (-N=N-NH-) produced by condensation of the aliphatic or aromatic amine with the carbonyl group, and they have different applications as chemical and biological reagents [13-16]. To the best of our

knowledge, few reports use triazene and its derivatives as metal corrosion inhibitors. The density functional theory DFT used to determine the molecular structure is used to determine the electronic structure, reactivity, and corrosion inhibitors efficiency [17, 18]. The DFT with the B3LYP functional is used to compare the different descriptors' effect on the compound's computed molecular properties understudy and inhibitor molecules visible on the metal's surface [19, 20]. Quantum chemical calculations of the triazene derivatives showed the more electron donating capacity [11]. In addition, the experimental results are confirmed and correlated with such theoretical calculations [10, 12, 21]. Many corrosion studies examine the corrosion inhibiting properties of compounds using the DFT/B3LYP method, and these studies showed a relationship between the calculated parameters and the inhibition efficiency [18, 22-24].

This work investigates triazene compounds' inhibition properties as novel corrosion inhibitors for mild steel in 1 M H_2SO_4 at various concentrations and temperatures using open circuit potential, electrochemical impedance spectroscopy, potentiodynamic polarization, scanning electron microscope, and theoretical investigations.

2. Materials and Methods

6

2.1. Triazene synthesis

Triazene compounds used as corrosion inhibitors have been previously synthesized throughout all the experiments reported by Reheim et al. [25, 26]. The molecular structures of inhibitors, abbreviated as T1, T2, and T3, respectively, are represented in Table 1.

Table 1 Molecular structure, names, abbreviations, formula, and weight of the triazene derivatives studied.

Code	Structure	Name	Formula and molecular weight
T1		4-(3-(1-ethoxy-1,3-dioxooctadecan-2-yl) triaz-1-enyl)-2-hydroxynaphthalene-1-sulphonic acid	$C_{31}H_{47}N_3O_7S$ 605.79
T2		Methyl 4-(3-(1-ethoxy-1,3-dioxooctadecan-2-yl) triaz-1-enyl)benzoate	$C_{28}H_{45}N_3O_5$ 503.67
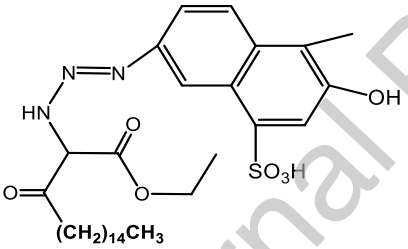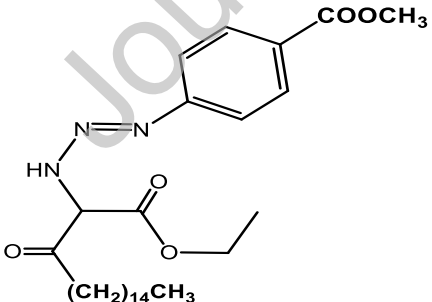
T3

Ethyl-3-oxo-2-(3-p-tolyl

triaz-2-nyl)octadecanoate

$C_{27}H_{45}N_3O_3$

459.66
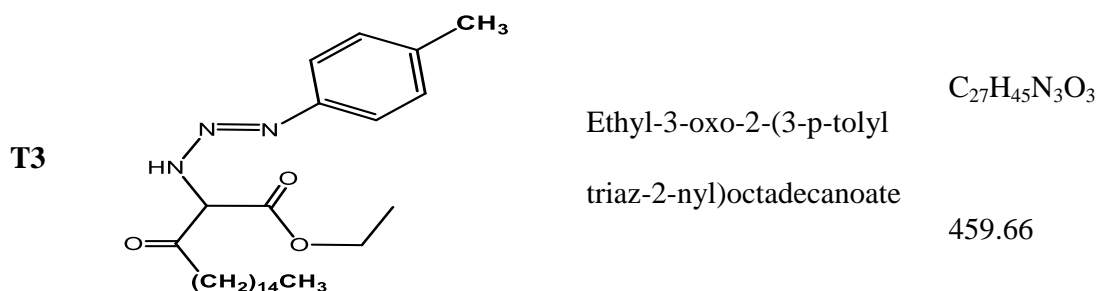
2.2. Mild steel electrode

The AL-EZZ Company equipped MS samples of dimension $2\times1\times0.1$ cm^3 used in Alexandria, and their composition is as follows (wt/wt%) Fe 98.74. Before the test, the specimens polished using emery paper SiC paper 1400 grade to obtain a smooth surface. Specimens degreased again with acetone and finally dried with air.

2.3. Corrosive and inhibitor concentrations

The corrosive media was H_2SO_4 (1 M, diluted by second distilled water) in 95-98% purity (Sigma–Aldrich Laborchemikalien. German). The inhibitors used herein were prepared at 50, 100, 200, and 500 ppm by analytical methods.

2.4. Electroanalysis cell

The electroanalysis cell used in this work consists of a working electrode (MS), reference electrode (Hg/Hg_2Cl_2), and counter electrode (Pt wire).

8

2.5. Electrochemical measurements

MS electrodes in 1 M H_2SO_4 without and with various triazene derivatives concentrations at different temperatures were studied electrochemically by open circuit potential (OCP) for 30 min. until a steady state was obtained potentiodynamic polarizations such as Tafel plots polarization (TP). The measurements were performed in a corrosion system with model 352/252, using EG & G potentiostat/galvanostat model 273A driven. TP applied ± 250 mV vs. E_{ocp} at 0.4 mV/s. Electrochemical impedance spectroscopy (EIS) was used to study MS electrodes' behavior after immersion time 2 h at 303 K with and without the inhibitor. The tests were performed by a model AUTO AC DSP device (ACM Instruments) in a frequency range of 100 kHz to 1 mHz [27].

2.6. Morphological study

A scanning electron microscope (SEM) was used to investigate the surface of MS before and after immersed in corrosive media in a presence inhibitor. SEM images proceed in the electronic microscope unit (JEOL, JSM5400LV).

2.7. Computed calculations

Gaussian 03W program package was used to compute the quantum chemical parameters [28]. Molecular geometries of used inhibitors were optimized by DFT

9

using Becke's three-parameter exchange functional (B3LYP) [29] and the 6-311G (d,p) basis set [30]. Quantum chemical descriptors such as the highest occupied molecular orbital (E_{HOMO}), the lowest unoccupied molecular orbital (E_{LUMO}), the energy gap (ΔE), the electron affinity (EA), the ionization potential (IP), the electronegativity (χ), the global hardness (η), the softness (σ), the electrophilicity index (ω), dipole moment (Dm by Debye), total energy (TE, a.u.) and the fraction of electrons transferred (ΔN) were calculated by the following equations (1-8) [10, 31-35]:

$$\Delta E = E_{LUMO} - E_{HOMO} \quad (1)$$

$$EA = -E_{LUMO} \quad (2)$$

$$IP = -E_{HOMO} \quad (3)$$

$$\chi = \frac{IP+EA}{2} \quad (4)$$

$$\eta = \frac{IP - EA}{2} \quad (5)$$

$$\sigma = \frac{1}{\eta} \quad (6)$$

$$\omega = \frac{\chi^2}{\eta} \quad (7)$$

$$\Delta N = \frac{[\chi Fe - \chi inh]}{2[\eta Fe + \eta inh]} \quad (8)$$

In equation (8), theoretical electronegativity and hardness values for iron were taken as $\chi_{Fe} \approx 7$ eV [33] and as $\eta_{Fe} = 0$, assuming that the IP equal the EA for bulk metals

10

[34]. Molecular electrostatic potential (MEP) maps and the contour plots for the inhibitors studied to determine nucleophilic and electrophilic active sites.

3. Results and Discussion

3.1. Electrochemical analysis

Open circuit voltage means no current ($I_{corr}= 0$) passes in the cell. Shifting in steady-state potential (E_{ss}) on the positive side shows a block of inhibitor on the anodic sites, while shifting E_{ss} in the negative potential indicates cathodic control. The E (mV) vs. time (min.) curves for T1, T2, and T3 compounds in 1 M H_2SO_4 for the MS electrode at 303 K presented in Fig. 1. It is clear from curves that the E_{ss} of electrode shift into observed positive potential than the blank solution (1 M H_2SO_4) for all inhibitor concentrations used. With the values of potentials shown in Table 2, it is clear that the formation of a layer of inhibitor adsorbed on the active anodic sites on the MS electrode surface correlated with the shifting of E_{ss} to a positive direction.
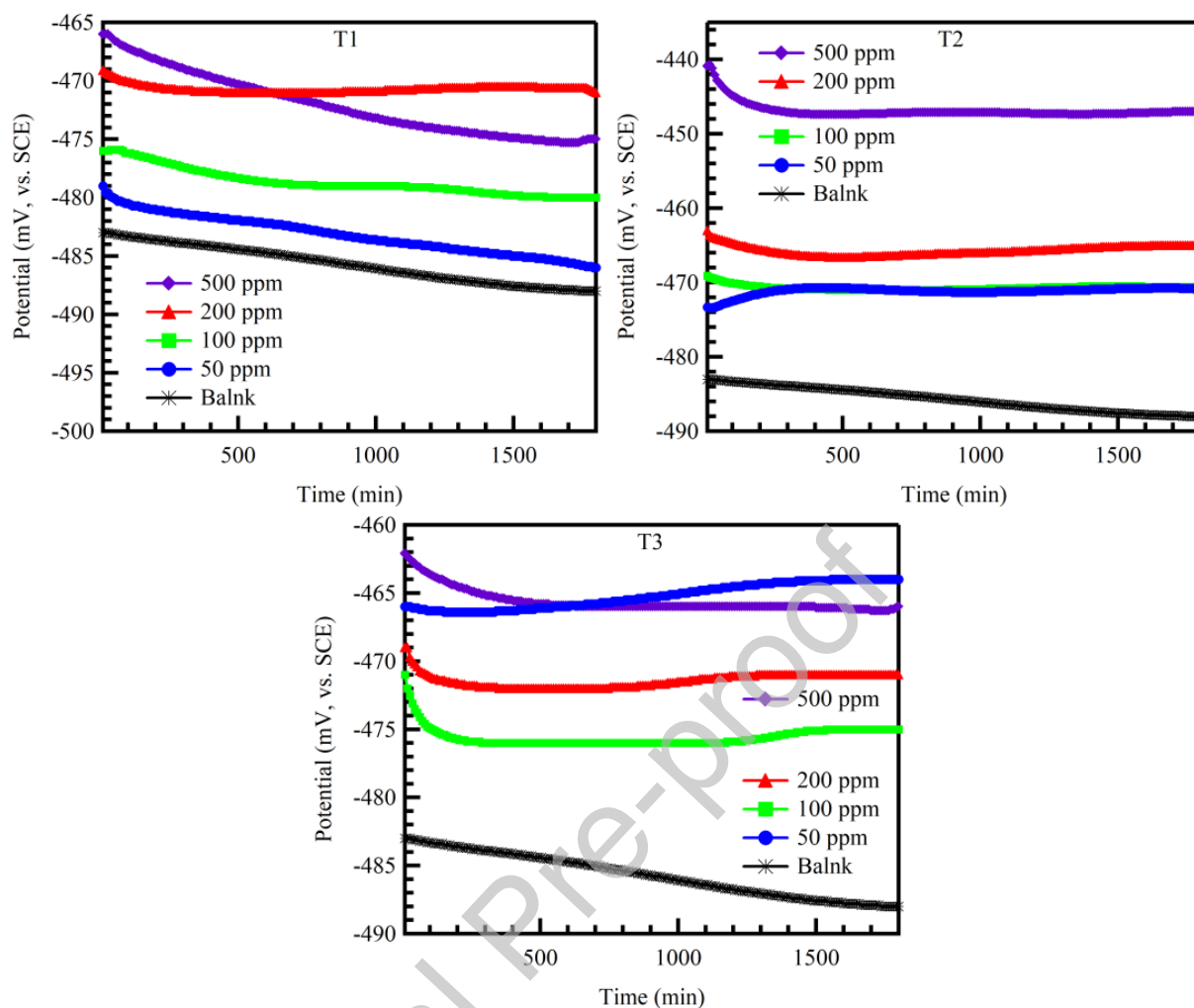
Fig. 1. Potential-time curves for mild steel at various concentrations of the triazene compounds at 303 K.

Table 2 Values of E_{im} and E_{ss} (mV) for mild steel at various temperatures of the triazene compounds.

Test solution	Conc. (ppm)	303 K		313 K		323 K		343 K	
		$-E_{im}$	$-E_{ss}$	$-E_{im}$	$-E_{ss}$	$-E_{im}$	$-E_{ss}$	$-E_{im}$	$-E_{ss}$
H_2SO_4	—	483	488	493	503	496	504	500	503

12

(1 M)									
	50	479	486	490	496	494	499	486	424
	100	486	485	494	500	493	501	510	501
T1	200	490	483	478	496	476	490	486	492
	500	476	480	497	501	486	493	510	502
	50	473	471	503	448	461	472	483	479
	100	469	471	469	462	505	471	456	459
T2	200	463	465	472	469	479	470	472	466
	500	440	447	456	449	469	464	486	486
	50	466	464	474	472	472	481	491	469
	100	471	475	485	483	466	475	516	503
T3	200	469	471	478	472	471	458	490	491
	500	462	466	490	468	472	463	513	469

Tafel polarization plots for MS without and with T1, T2, and T3 compounds at concentrations 50 to 500 ppm at different temperatures in 1 M H_2SO_4 solution are shown in Fig. 2. The corrosion parameters such as corrosion current (I_{corr}) potential (E_{corr}) rate (CR) and inhibition efficiency (IE, %) were tabulated in Tables 3-6. The values of CR, IE, and surface coverage (θ) were obtained using the equations (9-11) [36, 37]:

$$CR \ (mmy) = 0.13 \ I_{corr} \frac{(Eq.Wt)}{A \ \rho} \qquad (9)$$

13

Where Eq. Wt. is the equivalent weight of the metal, A is the area (cm^2), ρ is density (g/cm^3), and 0.13 is the metric and time conversion factor.

$$IE\ (\%) = \left[\frac{(CR_{without} - CR_{with})}{CR_{without}} \times 100\right] \qquad (10)$$

Where $CR_{without}$ and CR_{with} are the corrosion rate in absence and presence inhibitors, respectively.

$$\theta = \frac{IE}{100} \qquad (11)$$

Tafel polarization shown in Fig. 2 indicated that the anodic and cathodic reactions changed at different concentrations of triazene derivatives T1, T2, and T3. These mixed-type inhibitors indicate the reduction in the dissolution of the MS and retard of hydrogen evaluation [11, 12]. The values of E_{corr} presented in Tables 3-6 show the difference in recording E_{corr} without and with inhibitors less than 85 mV, confirming the mixed-type inhibition [12, 38-40].

In Tables 3-6, it observed that the T1 compound has the highest IE reach to 98.51% at 500 ppm at temperature 303 K, due to the presence of S, N, O as heterocyclic atoms and high molecular weight [41], also, presence of hydroxyl group gives T1 ability to adsorb and form protection layers on the surface of MS. In addition, the SO$_3$H group tends to donate its HOMO σ- or π-electrons to the appropriate vacant p-orbitals or d-orbitals of the metal atom [42]. On the other hand, the decrease of oxygen atoms in T2 and T3 indicates decreased IE compared with T1 compound. The order of IE of the triazene decreases in the following order: T1 > T2 > T3.

14

Temp. (K)	Test solution	Conc. (ppm)	R_P (Ω)	β_a (mV/dec)	β_c (mV/dec)	$-E_{corr}$ (mV)	i_{corr} ($\mu A/cm^2$)	CR (mpy)	$\eta.p$ (%)	θ
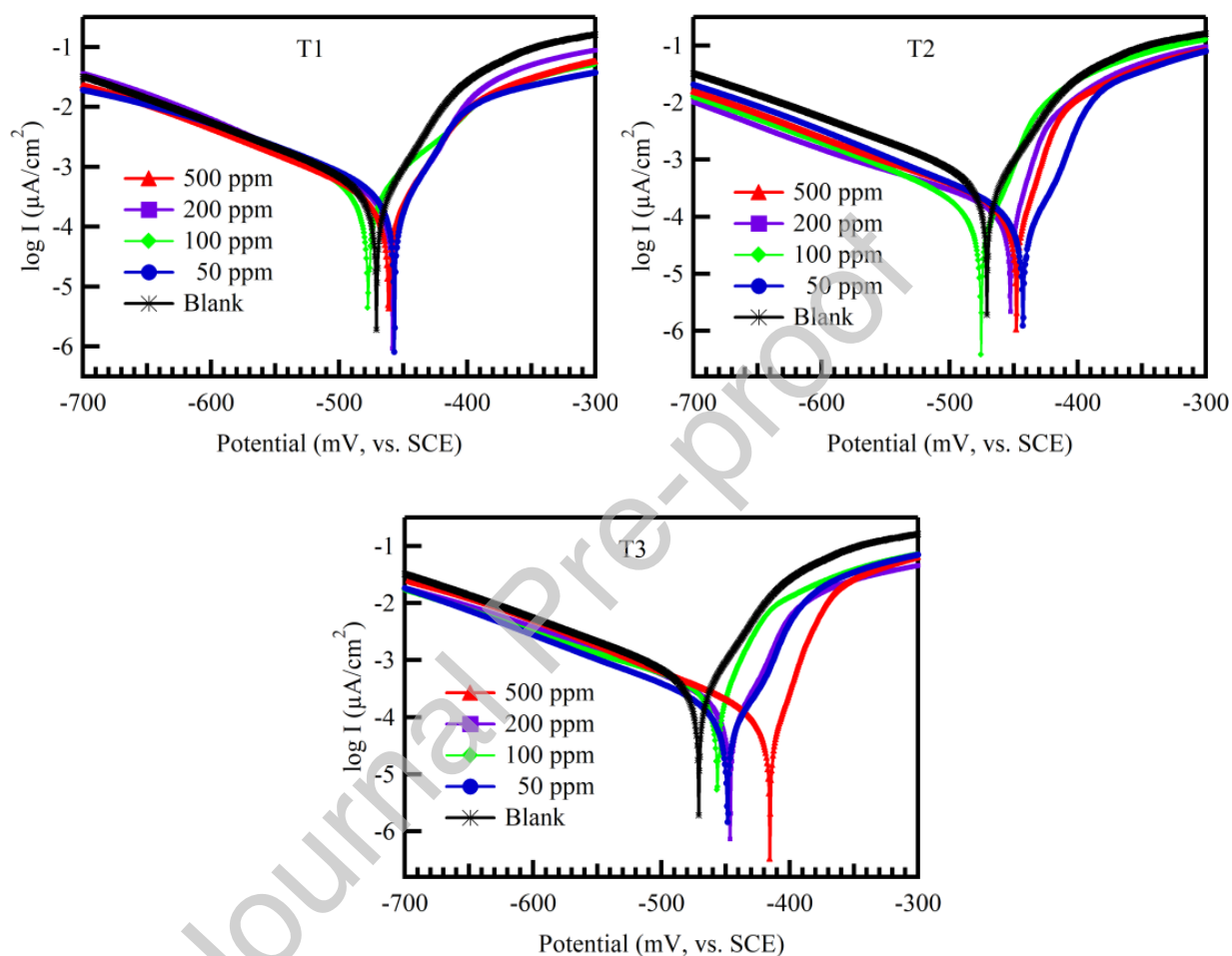
Fig. 2. Tafel plot polarization curves of mild steel at different triazene concentrations at 303 K.

Table 3 Potentiodynamic parameters of the triazene compounds at various temperatures.

15

Temp	Sample	Dose								
	H_2SO_4	—	40.12	82.58	142.6	471	718	662.02	—	—
	T1	50	55.14	30.63	53.77	457	170	157.11	76.27	0.76
		100	60.02	23.54	44.54	459	121	111.38	83.18	0.83
		200	69.30	15.82	32.43	465	61	56.06	91.53	0.92
		500	81.33	4.21	24.32	461	11	9.87	98.51	0.99
303	T2	50	50.99	70.54	130.51	490	220	203.22	69.30	0.69
		100	53.12	65.12	123.58	495	179	164.95	75.08	0.75
		200	57.19	58.96	101.45	493	102	93.59	85.86	0.86
		500	65.02	32.87	88.98	499	68	62.51	90.56	0.91
	T3	50	48.30	72.58	136.42	463	256	235.86	64.37	0.64
		100	51.02	65.87	125.44	466	188	173.71	73.76	0.74
		200	55.13	55.78	111.25	471	123	113.04	82.92	0.83
		500	59.12	25.64	96.51	469	98	90.54	86.32	0.86
	H_2SO_4	—	24.40	95.21	163.51	477	2080	1917.83	—	—
	T1	50	34.65	41.81	64.72	468	726	669.03	65.12	0.65
		100	37.13	33.42	55.14	470	581	535.43	72.08	0.72
		200	44.05	23.43	44.33	468	385	355.35	81.47	0.81
		500	50.13	17.78	32.42	474	178	163.94	91.45	0.91
313	T2	50	31.02	66.87	96.25	490	851	784.38	59.10	0.59
		100	33.02	54.12	89.48	488	713	657.23	65.73	0.66
		200	37.15	33.21	66.78	492	461	424.78	77.85	0.78
		500	42.18	19.12	44.58	492	312	287.49	85.01	0.85
	T3	50	30.30	89.78	113.47	500	888	818.31	57.33	0.57
		100	31.14	77.12	102.45	463	780	726.66	62.11	0.62
		200	35.22	63.45	88.78	465	520	479.83	74.98	0.75

		500	38.13	44.78	65.74	471	356	327.88	82.90	0.83
	H_2SO_4	—	13.65	121.14	200.74	471	5284	4872.04	—	—
	T1	50	21.16	79.33	165.35	466	2242	2067.02	57.57	0.58
		100	24.12	56.35	155.77	464	1879	1732.78	64.43	0.64
		200	28.17	44.87	132.72	461	1301	1199.38	75.38	0.75
		500	38.05	23.69	97.81	445	942	868.10	82.18	0.82
323	T2	50	19.04	101.25	122.54	497	2715	2503.14	48.62	0.49
		100	21.01	87.48	107.48	491	2342	2159.22	55.68	0.56
		200	24.15	75.18	103.58	495	1801	1660.49	65.92	0.66
		500	26.15	53.97	88.12	493	1321	1217.55	75.01	0.75
	T3	50	17.01	111.27	164.85	445	2855	2631.95	45.98	0.46
		100	20.03	88.47	143.72	463	2561	2361.15	51.54	0.52
		200	21.02	62.89	122.98	466	1998	1842.41	62.18	0.62
		500	25.44	32.84	99.98	473	1406	1296.11	73.40	0.73
	H_2SO_4	—	7.05	162.21	290.47	468	37260	34355.05	—	—
	T1	50	16.13	75.05	92.18	469	19885	18334.31	46.63	0.47
		100	20.20	68.51	88.25	462	15790	14558.48	57.62	0.58
		200	25.14	60.25	75.25	466	12355	11391.57	66.84	0.67
		500	30.05	56.99	76.69	460	8746	8063.94	76.53	0.77
343	T2	50	13.15	125.48	209.46	498	22114	20390.18	40.65	0.41
		100	16.01	105.24	188.65	492	19145	17652.56	48.62	0.49
		200	18.30	88.45	144.78	496	15125	13945.61	59.41	0.59
		500	23.03	63.78	113.46	492	11846	10921.98	68.21	0.68
	T3	50	12.13	133.47	225.87	466	22788	21011.08	38.84	0.39
		100	15.09	117.82	204.7	462	20145	18574.50	45.93	0.46

200	16.05	99.45	185.4	465	15663	14441.75	57.96	0.58
500	20.13	75.41	133.82	471	12334	11372.11	66.90	0.67

Solution resistance (R_s), charge-transfer resistance (R_{ct}), double-layer capacitance (C_{dl}), θ and IE for MS corrosion without and with different concentrations of T1, T2, and T3 compounds in 1 M H_2SO_4 solution at room temperature were calculated using the following equations (12, 13) [43]:

$$\text{IE (\%)} = \left[\frac{R_{ct(with)} - R_{ct(without)}}{R_{ct(with)}}\right] \times 100 \qquad (12)$$

Where, R_{ct} (with) and R_{ct} (without) are the charge transfer resistances in the presence and absence of inhibitor, respectively.

$$C_{dl} = \left(Y_0\, R_{ct}^{1-n}\right)^{\frac{1}{n}} \qquad (13)$$

Y_0 is the constant phase element, and n is the exponent [43]. The value of n represents the deviation from the ideal behavior, and it lies between 0 and 1. Figure 3 presented that the inhibitor addition does not alter the impedance semicircle curve of the Nyquist plots. The impedance curve showed one capacitive loop; however, the capacitive loop's diameter increases with T1 > T2 > T3. Impedance data were fitted using the equivalent circuit model shown in Fig. 3, which includes Rs and C_{dl} and R_{ct}. From Table 4, R_{ct} increases and C_{dl} decreases compared to that obtained with a blank solution. The adsorption of the inhibitor molecules on the metal surface forms a protective layer that decreases the double layer thickness; therefore, R_{ct}

18

values increase, and C_{dl} values decrease [44]. In addition, this also indicates that the inhibitor molecules were absorbed in the metal/solution interface [45].
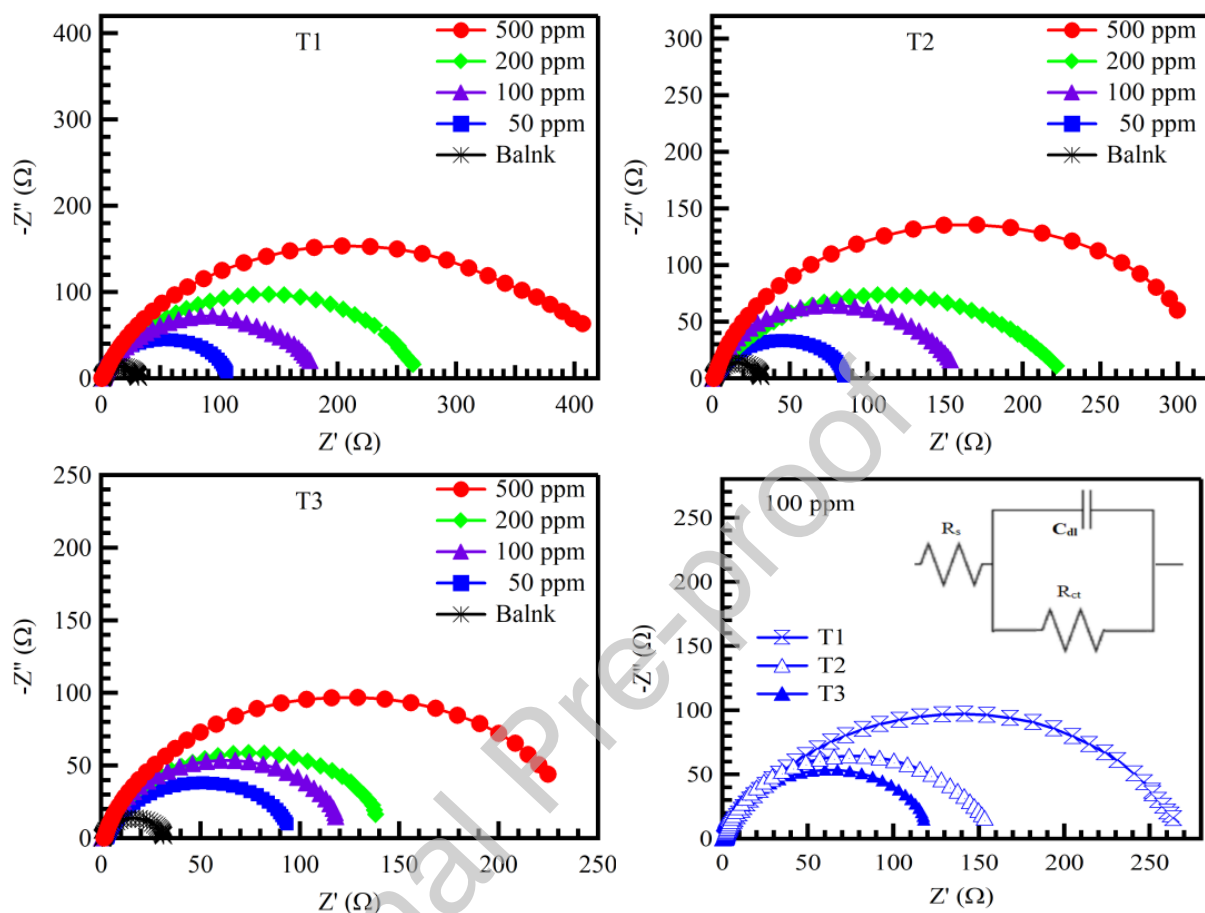
Fig. 3. Nyquist plots for mild steel at different triazene concentrations at 303 K: The inset is the equivalent circuit.

Table 4 Impedance data for mild steel without and with different concentrations of triazene compounds at 303 K.

19

Test solution	Conc. (ppm)	R_{sol} (Ω/cm^2)	R_{ct} (Ω/cm^2)	Y_0 ($\mu F/cm^2$)	n	C_{dl} ($\mu F/cm^2$)	$\eta._I$ (%)	θ
H_2SO_4	-	0.581	30.94	724	0.90	482.17	-	-
	50	0.585	109.7	558	0.93	449.86	71.80	0.72
	100	1.767	180.3	284	0.87	183.62	82.81	0.83
T1	200	1.635	262.3	430	0.83	275.77	88.20	0.88
	500	0.641	449.1	257	0.82	161.23	93.11	0.93
	50	0.430	98.7	294	0.94	238.15	68.65	0.69
	100	0.623	153.7	284	0.87	186.68	79.87	0.80
T2	200	0.787	215.3	160	0.76	54.78	85.60	0.86
	500	1.038	313.4	264	0.88	186.39	90.13	0.90
	50	2.991	91.11	416	0.86	244.45	66.04	0.66
	100	0.597	114.5	305	0.89	201.01	72.98	0.73
T3	200	1.595	147.9	304	0.88	195.11	79.08	0.79
	500	1.574	235.3	278	0.88	192.04	86.85	0.87

3.2. Thermodynamic activation calculations

The activation energy (E_a) is the minimum energy required for a successful molecular collision. The relationships between the temperatures and IE of an inhibitor and E_a have three types according to temperature effects. IE decreases with the increase in temperature, E_a (presence inhibitors) > E_a (absence inhibitors), IE increases with the increase in temperature, E_a (presence inhibitors) < E_a (absence inhibitors), or IE does not change with temperature, E_a (presence solution) = E_a (absence inhibitors) [46].

The activation energies for the corrosion of MS in the absence and presence of the inhibitors were calculated using the Arrhenius equation (14) [47]:

$$\text{Log } CR = \frac{-E_a}{2.303RT} + \log A \qquad (14)$$

Where E_a is the activation energy for the reaction, R is the gas constant, and A is the Arrhenius pre-exponential factor.

Arrhenius plot of log CR against 1/T for MS in the absence and presence of different concentrations of compounds T1, T2, and T3 at temperatures 303, 313, 323, and 343 K were shown graphically in Fig. 4, gave straight lines with a slope of –E_a/2.303R. Table 5 shows that E_a values for inhibited solutions are higher than those for the uninhibited solution, suggesting a slow dissolution process of MS (lower corrosion rate). This results from the formation of a film on the MS surface serving as an energy barrier for the MS corrosion, and it can be interpreted as an indication of physical adsorption [48, 49]. The adsorption of T1, T2, and T3 compounds on the MS surface is consistent with the inhibitor's charge transfer mechanism to the MS surface. The enthalpy (ΔH) and entropy (ΔS) of activation were calculated using equation (15) [47]:

$$CR = \frac{RT}{Nh} \exp\left(\frac{\Delta S}{R}\right) \exp\left(-\frac{\Delta H}{RT}\right) \qquad (15)$$

Where h is Planck's constant and N_A is Avogadro's number.

From Table 5, the positive values of ΔH indicate the endothermic process of MS dissolution process. The data of ΔS with inhibitors were higher than without it; this

21

indicates that an increase in randomness occurred on going from reactants to the activated complex. The adsorption of T1, T2, and T3 compounds from the sulphuric acid solution could be a substitution process between T1, T2, and T3 compounds in the aqueous phase and water molecules at the electrode surface [50]. In this case, the adsorption of T1, T2, and T3 compounds was accompanied by water molecules' desorption from the surface. Thus, the increase in ΔS of activation was attributed to increasing solvent entropy [51].
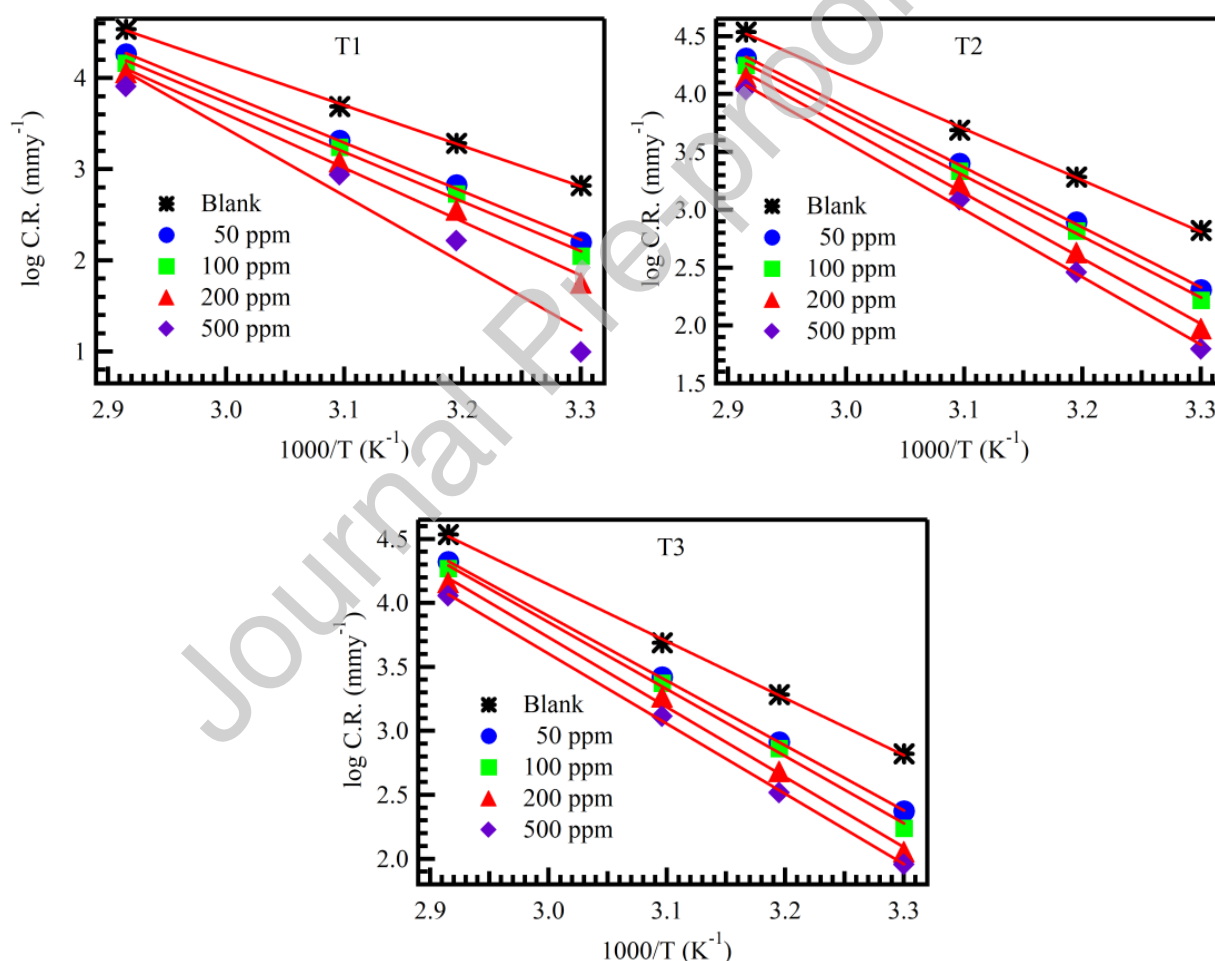
Fig. 4. Arrhenius plots for mild steel dissolution in different concentrations of T1, T2, and T3 solutions.

22

Table 5 Activation parameters values for mild steel in different concentrations of the triazene compounds.

Tested solution	Conc. (ppm)	E_a^* (KJ/mol)	ΔH^* (kJ/mol)	ΔS^* (Jmol/k)
H$_2$SO$_4$	-	85.13	82.45	80.83
T1	50	101.96	99.28	125.20
	100	104.13	101.45	129.92
	200	112.82	110.14	153.57
	500	140.93	138.25	234.82
T2	50	99.16	96.47	117.88
	100	100.53	97.85	120.77
	200	107.80	105.12	140.42
	500	111.50	108.82	149.13
T3	50	96.99	94.30	111.70
	100	100.30	97.61	120.64
	200	104.64	101.96	131.48
	500	106.23	102.31	130.06

3.3. Adsorption isotherm

Calculation of adsorption isotherm is one of the crucial methods that represent the interaction between the molecules of inhibitor and metal surface; the Langmuir model agrees more with the experimental results obtained in this study by applying the following equation (16) [52]:

$$\frac{C}{\theta} = \frac{1}{K_{ads}} + C \qquad (16)$$

Adsorption free energy ΔG_{ads} can be calculated by using equation (17) [49]:

$$\Delta G_{ads} = -2.303RT \log(55.5K) \qquad (17)$$

Where, 55.5 is the molar concentration of water in the solution, T is the absolute temperature.

The ΔG_{ads} of T1, T2, and T3 compounds of MS in 1 M H_2SO_4 at 303, 313, 323, and 343 K were calculated using slopes of the lines and the ordinate axis intercept the straight lines as shown in Fig. 5. The deducted values are summarized in Table 6. ΔG_{ads} values obey physical adsorption isotherm, which has ranged from -16.49 to -19.59 kJ/mol for all tested compounds with their different concentrations.

The adsorption heat was calculated according to the Van't Hoff equation (18) [53]:

$$\log K_{ads} = (\frac{\Delta H_{ads}}{RT}) + \text{Const.} \qquad (18)$$

Where ΔH_{ads} and K_{ads} are the adsorption heat and adsorptive equilibrium constant, respectively. It is noted that $\Delta H_{ads}/R$ is the straight-line slope for plotting log K_{ads} against 1000/T (Fig. 5). The positive values of ΔH_{ads} show that the adsorption of the inhibitors is an endothermic process [50, 54]. ΔS_{ads} can be calculated using the following equation (19).

$$\Delta G_{ads} = \Delta H_{ads} - T\Delta S_{ads} \qquad (19)$$

24

It is clear from results that ΔS_{ads} positive values in the presence of T1, T2, and T3 compounds, which an ordered layer may explain onto the MS surface. Sads' positive value is attributed to the increase of disorder due to triazene molecules' adsorption by desorption of more water molecules.
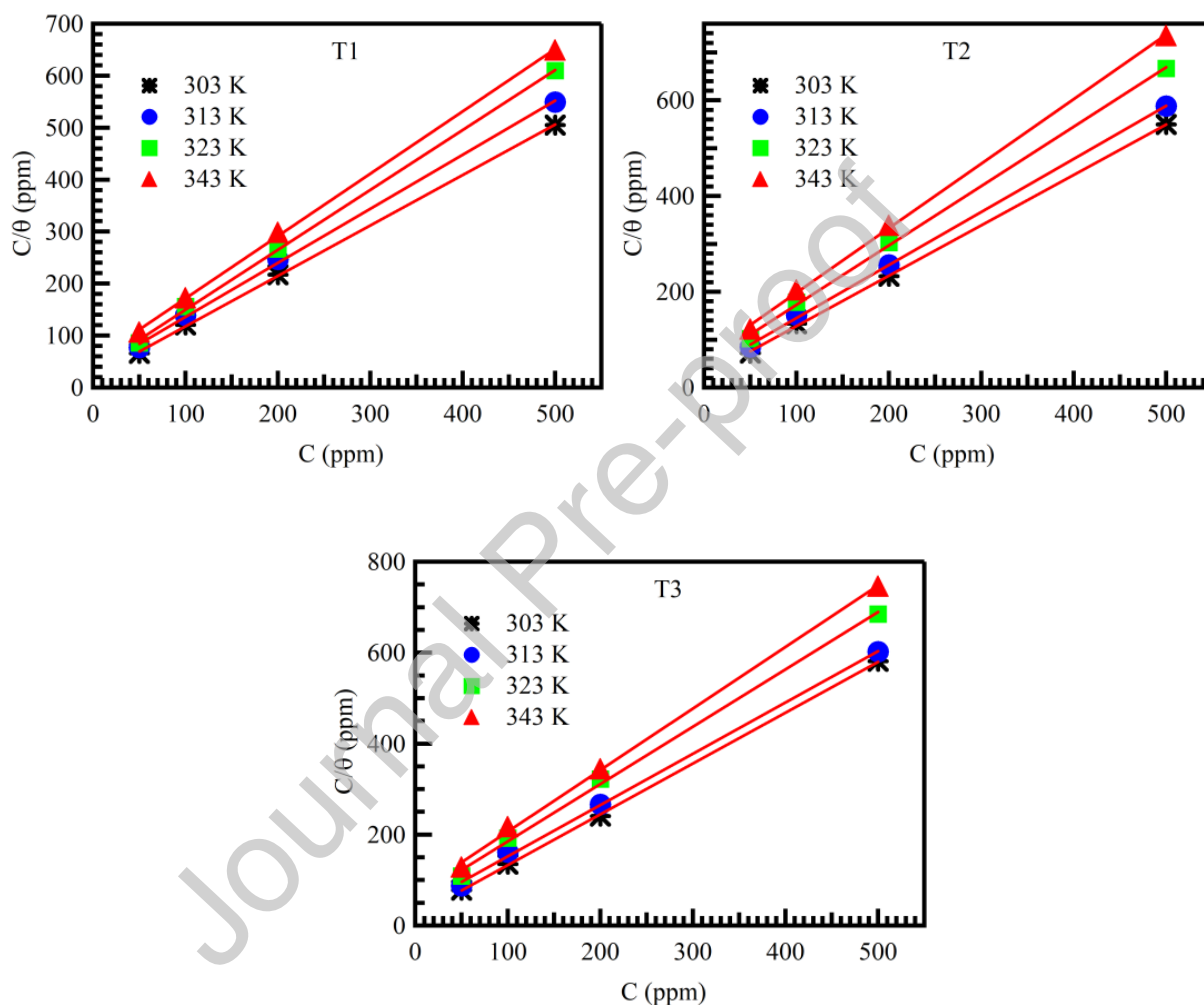
Fig. 5. Langmuir isotherm of the triazene adsorption on mild steel at different temperatures.

Table 6 Thermodynamic parameters using Langmuir adsorption on mild steel surface containing different triazene compounds at different temperatures.

Tested solution	T (K)	Log K_{ads}	$-\Delta G_{ads}$ (kJ/mol)	ΔS_{ads} (J/mol K)	ΔH_{ads} (kJ/mol K)
T1	303	1.69	-19.59	91.49	
	313	1.50	-18.48	85.02	
	323	1.46	-18.26	81.70	8.13
	343	1.29	-17.30	74.14	
T2	303	1.63	-19.27	75.97	
	313	1.46	-18.28	70.38	
	323	1.31	-17.43	65.57	3.75
	343	1.45	-18.20	63.99	
T3	303	1.67	-19.48	100.76	
	313	1.40	-17.94	92.62	
	323	1.23	-16.95	86.69	11.05
	343	1.14	-16.49	80.29	

3.4. Morphological analysis

Fig. 6a illustrates the surface morphology of a polished MS electrode before exposure to corrosion media. The micrograph is shown in Fig. 6b; the polished

26

specimen was kept in the blank solution 1 M H_2SO_4 for 24 h; the micrograph revealed that the surface was strongly damaged in the absence of inhibitor. Fig. 6(c, d, and e) shows specimen which was kept in 1 M H_2SO_4 at 500 ppm of inhibitor solution of some organic triazene compounds corresponding to the values of IE T1, T2, and T3 respectively at 24 h, depends upon the concentration of the inhibitor solution, suggesting that the presence of an adsorbed layer of the inhibitor on MS surface which impedes the corrosion rate of metal appreciably.
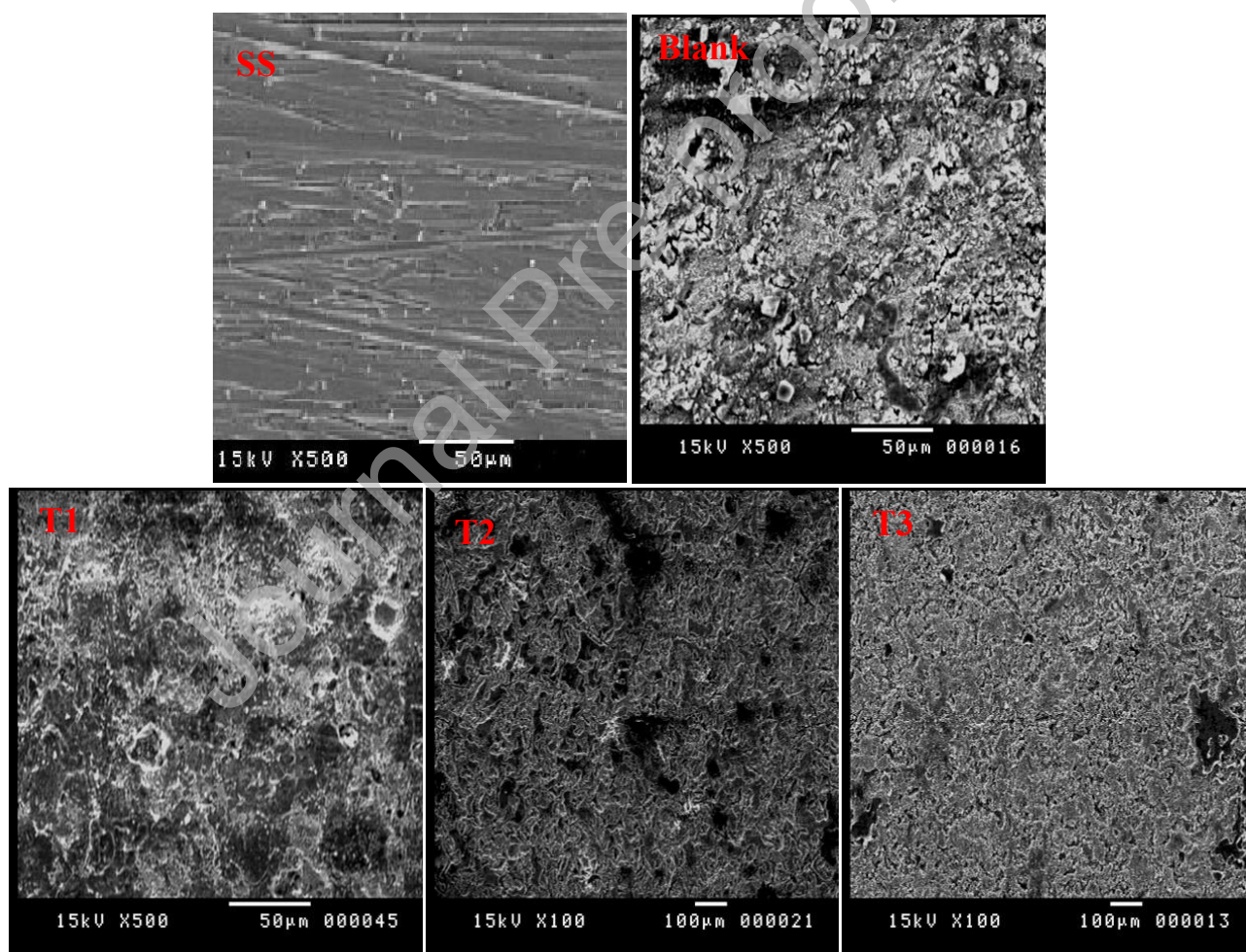
Fig. 6. Scanning electron micrographs of mild steel surface after 24 h immersed at room temperature without and with 500 ppm of T1, T2, and T3.

3.6. Quantum chemical calculations

The optimized geometries of T1, T2, and T3 in the form, including its HOMO and LUMO distributions shown in Fig. 7, show that T1, T2, and T3 have similar HOMO and LUMO distributions, which were all located on the entire inhibitor moiety. The HOMO and LUMO of T1, T2, and T3 have mainly located around the (C, N, and O) moiety. The presence of nitrogen and oxygen atoms and several π-electrons on these molecules ensures strong adsorption of the MS surface inhibitors.

Table 7 lists the theoretical results revealed by increasing EH values and decreasing the value of EL, which is in good agreement with results obtained from experiments. The calculations results showed that that T1, with the highest corrosion inhibition efficiency among the investigated compounds, has the highest E_H and lowest E_L; on the other hand, a lower value of the energy gap $\Delta E = E_L - E_H$ is good inhibition efficiency because the energy to remove an electron to last occupied molecular orbital will be low [55]. In Table 7, it was clear that the order of decreasing of ΔE from where the prediction of actives and the best inhibition compounds to limit the corrosion of metals (2.36 < 2.85 < 3.13) for compounds (T1, T2, and T3) with the molecule increases leading to increase in the average of IE (87.37% > 80.21% > 76.84%), respectively.

The electron affinity of molecules is a complicated function of their electronic structure. The E_L is directly related to the electron affinity. Table 7 illustrates a good correlation between the electron affinity and the η.p values for the compounds. The

28

order of increasing the electron affinity values is 5.25 <5.56 < 5.85, with increasing average the η.p of 76.84% > 80.21% > 87.37% for T3, T2 and T1 compounds. The electron affinity increased along with each series, the affinity of the inhibitor to accept electrons from the MS surface into the inhibitor antibonding orbital increase, and the energy is given off increases. The η.p increase, indicating more protection for the MS surface [56]. Electronegativity was also calculated and showed some agreement with the experimental results.

A high value of absolute hardness indicates high stability and low reactivity for a molecule [56]. It was clear from Table 7 that as the hardness values increase, the IE values decrease for investigated inhibitors. The inhibitor T3 has the highest hardness (η=1.57) and the minimum IE value (76.84). The inhibitor T1 has the lowest hardness (η=1.18) and the maximum IE value (87.37). The values of increasing hardness are in good agreement with the experimental IE values. Soft molecules are more interactive than rigid molecules because a soft molecule has a lower ΔE [57] from Table 7, it was clear that as the softness values increased, the IE values increased for investigated inhibitors. The inhibitor T1 has the highest softness (σ=0.85) and the maximum IE value (87.37%). The inhibitor T3 has the lowest softness (σ=0.64) and the minimum IE value (76.84). The values of increasing softness are in good agreement with the experimental IE values.

The molecule's nucleophilicity or electrophilicity could be identified from the electrophilicity index values. The high values of ω refer to the molecule's tendency

29

to act as an electrophile, while the low values of ω indicate that the molecule tends to act as a nucleophile [58]. From Table 7, the electrophilicity values increase as follows: (29.68 < 34.23 < 42.01 eV) comparing electrophilicity index values with the IE_{exp} (87.37% > 80.21% > 76.84%) for T1, T2 and T3 compounds, respectively.

The inhibition efficiency increases with increasing the dipole moment's value, depending on the type and nature of molecules used [59]. Table 7 showed that the values of IE increased with the increasing μ values. The inhibitor T1 has the highest μ value (9.44 D) and the maximum IE value (87.37%), and T3 has the lowest μ value (3.59 D) and the minimum IE value (76.84%).

The inhibitor negative centers are responsible for molecule adsorption on MS surface; so, the TNC is an essential factor in determining its inhibition efficiency. As TNC increases, inhibition efficiency increases. The calculated values of TNC showed that T1 has the highest TNC of -7.54, compared to T2 (-6.19) and T3 (-5.63).

The total energy (TE) equal to ∑(internal, potential, and kinetic energy). According to Hohenberg and Kohn [60], The minimum value of TE functional is the ground state energy of the system. The electronic charge density, which yields this minimum, is then the same single-particle ground state energy. Table 7 showed that TE values are -1446.28, -1634.88 and -2299.07 a.m.u) for (T3, T2 and T1), respectively. The values of IE increased with the increase of TE values. The T1 inhibitor has the highest TE value and the maximum IE value (87.37%). The

inhibitor T3 has the lowest TE value and the minimum IE value (76.84%). From these results, it was clear that there was a good agreement between experimental IE and theoretical TE data. The high TE values confirm the higher stability of the molecule and consequently lower donating ability.

The values of χ and η obtained were used to calculate the fraction of electrons transferred from the inhibitor to the metal surface (ΔN). If bulk MS and the inhibitor molecule are found together, the flow of electrons will occur from the molecule of lower electronegativity to the MS that has a higher electronegativity until the value of the chemical potential the same value [33, 61-64]. By Lukovits's study, if the value of $\Delta N < 3.6$, the IE increase by increasing the inhibitor's electron-donating ability on the metal surface [65]. From Table 7, generally, ΔN ranges from -0.014 to 0.005. T1 indicates the maximum transfer of electrons and greater IE. Thus, the fraction of transferred electrons is the largest for T1 as compared with other inhibitors studied.

Table 7 The obtained parameter values of the triazene compounds using B3LYP/6-311G (d,p) basis set method.

Comp.	E_H (ev)	E_L (ev)	ΔE (ev)	EA (ev)	IP (ev)	X (ev)	η (ev)	σ (ev)	ω (ev)	Dm (Debye)	TNC	TE (a.m.u)	ΔN (ev)	$(\eta.p)^*$ %
T1	-8.21	-5.85	2.36	5.85	8.21	7.03	1.18	0.85	42.01	9.44	-7.54	-2299.07	-0.01	87.37

31

T2	-8.41	-5.56	2.85	5.56	8.41	6.99	1.42	0.70	34.23	4.18	-6.19	-1634.88	0.01	80.21
T3	-8.38	-5.25	3.13	5.25	8.38	6.82	1.57	0.64	29.68	3.59	-5.63	-1446.28	0.06	76.84

*Average η.p values for different concentrations at room temperature

Comp.	Optimized structure	HOMO	LUMO
T1			
T2			
T3			
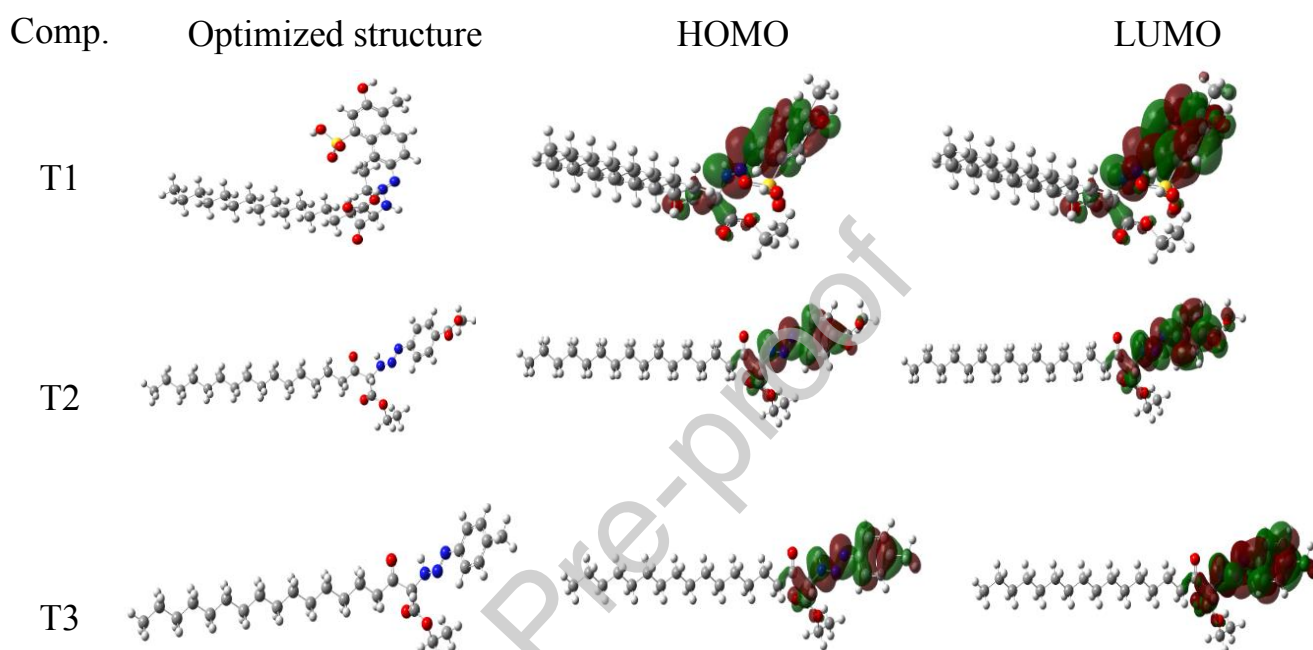
Fig. 7. Optimized molecular structure, HOMO, LUMO, and total charge density of the investigated T1, T2, and T3 compounds using (DFT) 6-311G (d, p) basis set method.

The MEP maps and contours show the molecular charge distribution and give information regarding reactive sites (size, shape, charge density, and reactive sites of organic molecules) for electrophilic and nucleophilic attack. Therefore, the binding mechanism between the organic molecules and the metal surface could be understood. The negative (red) regions of MEP indicate nucleophilic reactivity, but

32

the positive (blue) regions indicate electrophilic reactivity. Figure 8 shows the blue color around the C atom of the C=O group to which the pentadactyl chain is attached is dominated; hence this C atom has electrophilic reactivity. The total negative charges (TNC) of selected atoms (carbon, oxygen, and nitrogen) are recorded in Table 7. It was observed that T1 interacts with the metal surface more than T2 and T3. MEP maps shown in Fig. 8, there is the color red that indicates negative charge. The steric effect deduced from the MEP contour shown in Fig. 8 shows that the O atom of the other C=O group common to all inhibitors is the active site with less steric effect. Very high correlations were found between some parameters (ΔE, η, σ, ω, Dm, TE, and TNC) against IE_{exp}.
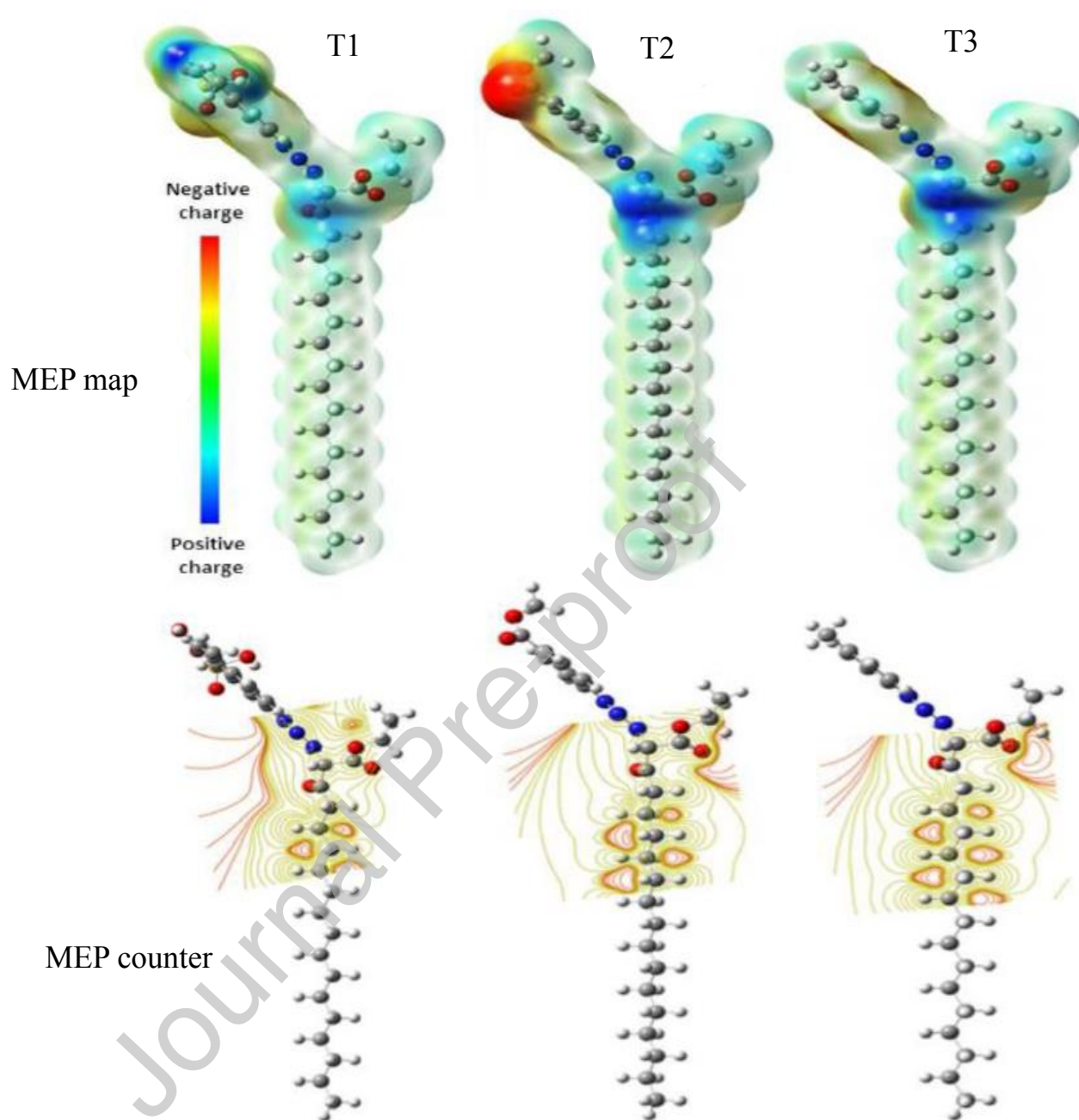
Fig. 8. Molecular electrostatic potential maps and contours of studied inhibitors at B3LYP method with 6-311G (d,p) basis set.

4. Conclusions

The experimental and theoretical results show that triazene compounds (T1, T2, T3) act as effective MS corrosion inhibitors in 1 M H_2SO_4. The compound with maximum inhibition activity is T1 (98.51%), while the minimum active compound is T3 (86.32 %) at room temperature. It is seen that η.p value of the compounds increases with increasing concentration but decreases with increasing temperature. The triazene compounds adsorption on MS surface from 1 M H_2SO_4 is a physical phenomenon proposed from the values of kinetic/thermodynamics parameters (E_a, ΔG_{ads}) obtained and obeys Langmuir adsorption isotherm. SEM analyzed the surface morphology. It gives a visual idea about forming a protective layer on the MS surface, which retards the CR. Some quantum chemical parameters, which will assist in the interpretation of the inhibition process, were calculated. Parameters were found to be closely related to the inhibition efficiencies of the inhibitors studied. The correlation graphs were obtained between the experimental inhibition efficiency and some parameters. The experimental and theoretical results were in good agreement.

CRediT author statement

M. H. Mahross: Conceptualization, Methodology, Software, Supervision. **Mahmoud A. Taher:** Supervision. **M. A. Mostfa:** Methodology, Writing- Original draft preparation. **Kwok Feng Chong:** Supervision, Writing -

Review & Editing. **Gomaa A.M. Ali:** Formal analysis, Supervision, Writing - Review & Editing, Validation.

Declaration of interests

The authors declare that they have no known competing financial interests or personal

relationships that could have appeared to influence the work reported in this paper.

References

[1] A.Y. El-Etre, M. Abdallah, Z.E. El-Tantawy, Corrosion inhibition of some metals using lawsonia extract, Corros. Sci. 47(2) (2005) 385-395, doi: https://doi.org/10.1016/j.corsci.2004.06.006.

[2] B.M. Prasanna, B.M. Praveen, N. Hebbar, T.V. Venkatesha, H.C. Tandon, Inhibition study of mild steel corrosion in 1 M hydrochloric acid solution by 2-chloro 3-formyl quinoline, Int. J. Ind. Chem. 7(1) (2015) 9-19, doi: https://doi.org/10.1007/s40090-015-0064-6.

[3] A.S. Fouda, M.A. Elmorsi, T. Fayed, I.A. El said, Oxazole derivatives as corrosion inhibitors for 316L stainless steel in sulfamic acid solutions, Desalin. Water Treat. (2014) 1-15, doi: https://doi.org/10.1080/19443994.2014.993717.

[4] N.H. Abu Bakar, G.A.M. Ali, J. Ismail, H. Algarni, K.F. Chong, Size-dependent corrosion behavior of graphene oxide coating, Prog. Org. Coat. 134 (2019) 272-280, doi: https://doi.org/10.1016/j.porgcoat.2019.05.011.

[5] D.S. Chauhan, M.A. Quraishi, V. Srivastava, J. Haque, B.E. ibrahimi, Virgin and chemically functionalized amino acids as green corrosion inhibitors: Influence of molecular structure through experimental and in silico studies, J. Mol. Struct. 1226 (2021) 129259, doi: https://doi.org/10.1016/j.molstruc.2020.129259.

[6] M.A. Ameer, A.M. Fekry, Inhibition effect of newly synthesized heterocyclic organic molecules on corrosion of steel in alkaline medium containing chloride, Int. J. Hydrogen Energy 35(20) (2010) 11387-11396, doi: https://doi.org/10.1016/j.ijhydene.2010.07.071.

[7] F.M. Bayoumi, W.A. Ghanem, Corrosion inhibition of mild steel using naphthalene disulfonic acid, Mater. Lett. 59(29-30) (2005) 3806-3809, doi: https://doi.org/10.1016/j.matlet.2005.06.070.

[8] M.A. Mostfa, H. Gomaa, I.M.M. Othman, G.A.M. Ali, Experimental and theoretical studies of a novel synthesized azopyrazole-benzenesulfonamide derivative as an efficient corrosion inhibitor for mild steel, J. Iran. Chem. Soc. (2020), doi: https://doi.org/10.1007/s13738-020-02106-7.

[9] D.S. Chauhan, C. Verma, M.A. Quraishi, Molecular structural aspects of organic corrosion inhibitors: Experimental and computational insights, J. Mol. Struct. 1227 (2021) 129374, doi: https://doi.org/10.1016/j.molstruc.2020.129374.

[10] P. Dohare, M.A. Quraishi, I.B. Obot, A combined electrochemical and theoretical study of pyridine-based Schiff bases as novel corrosion inhibitors for mild steel in hydrochloric acid medium, J. Chem. Sci. (Bangalore, India) 130(1) (2018) 8, doi: https://doi.org/10.1007/s12039-017-1408-x.

[11] A. Singh, K.R. Ansari, J. Haque, P. Dohare, H. Lgaz, R. Salghi, M.A. Quraishi, Effect of electron donating functional groups on corrosion inhibition of mild steel in hydrochloric acid: Experimental and quantum chemical study, Journal of the Taiwan

37

Institute of Chemical Engineers 82 (2018) 233-251, doi: https://doi.org/10.1016/j.jtice.2017.09.021.

[12] A. Nahlé, R. Salim, F. El Hajjaji, M. Aouad, M. Messali, E. Ech-Chihbi, B. Hammouti, M. Taleb, Novel triazole derivatives as ecological corrosion inhibitors for mild steel in 1.0 M HCl: experimental & theoretical approach, RSC Adv. 11(7) (2021) 4147-4162, doi: https://doi.org/10.1039/D0RA09679B.

[13] F. Zucchi, G. Trabanelli, C. Monticelli, The inhibition of copper corrosion in 0.1 M NaCl under heat exchange conditions, Corros. Sci. 38(1) (1996) 147-154, doi: https://doi.org/10.1016/0010-938x(96)00121-7.

[14] J.P. Chopart, J. Douglade, P. Fricoteaux, A. Olivier, Electrodeposition and electrodissolution of copper with a magnetic field: dynamic and stationary investigations, Electrochim. Acta 36(3-4) (1991) 459-463, doi: https://doi.org/10.1016/0013-4686(91)85128-t.

[15] M. Urquidi- Macdonald, S. Real, D.D. Macdonald, Application of Kramers-Kronig transforms in the analysis of electrochemical impedance data: II Transformations in the complex plane, J. Electrochem. Soc. 133(10) (1986) 2018-2024, doi: https://doi.org/10.1149/1.2108332.

[16] A.J.R.W.A. dos Santos, P. Bersch, H.P.M. de Oliveira, M. Hörner, G.L. Paraginski, Triazene 1-oxide compounds: Synthesis, characterization and evaluation as fluorescence sensor for biological applications, J. Mol. Struct. 1060 (2014) 264-271, doi: https://doi.org/10.1016/j.molstruc.2013.12.055.

[17] A. Ehsani, R. Moshrefi, M. Ahmadi, Electrochemical Investigation of Inhibitory of New Synthesized 3-(4-Iodophenyl)-2-Imino-2,3-Dihydrobenzo[d]Oxazol-5-yl 4-Methylbenzenesulfonate on Corrosion of Stainless Steel in Acidic Medium, J. Electrochem. Sci. Technol. 6(1) (2015) 7-15, doi: https://doi.org/10.33961/jecst.2015.6.1.15.

[18] K. Efil, I.B. Obot, Quantum chemical investigation of the relationship between molecular structure and corrosion inhibition efficiency of benzotriazole and its alkyl-derivatives on iron, Prot. Met. Phys. Chem. Surf. 53(6) (2017) 1139-1149, doi: https://doi.org/10.1134/s2070205118010215.

[19] E.E. Ebenso, T. Arslan, F. Kandemirli, N. Caner, I. Love, Quantum chemical studies of some rhodanine azosulpha drugs as corrosion inhibitors for mild steel in acidic medium, Int. J. Quantum Chem. 110(5) (2009) 1003-1018, doi: https://doi.org/10.1002/qua.22249.

[20] P. Senet, Chemical hardnesses of atoms and molecules from frontier orbitals, Chem. Phys. Lett. 275(5-6) (1997) 527-532, doi: https://doi.org/10.1016/s0009-2614(97)00799-9.

[21] T.S. Gaaz, R.M. Dakhil, D.M. Jamil, A.A. Al-Amiery, A.A. Kadhum, M. Takriff, Evaluation of green corrosion inhibition by extracts of citrus aurantium leaves against carbon steel in 1 M HCl medium complemented with quantum chemical assessment, Int. J. Thin Film Sci. Technol. 9(3) (2020) 171-179, doi: https://doi.org/10.18576/ijtfst/090307.

[22] N. Obi-Egbedi, I. Obot, M. El-Khaiary, S. Umoren, E. Ebenso, Computational simulation and statistical analysis on the relationship between corrosion inhibition efficiency and molecular structure of some phenanthroline derivatives on mild steel surface, Int. J. Electrochem. Sci. 6(5649) (2011) e5675.

[23] K. Efil, Y. Bekdemir, Theoretical study on corrosion inhibitory action of some aromatic imines with sulphanilic acid: A DFT study, Canadian Chem. Trans. 3(1) (2015) 85-93, doi: https://doi.org/10.13179/canchemtrans.2015.03.01.0165.

[24] F. Kayadibi, S.G. Sagdinc, Y.S. Kara, Density functional theory studies on the corrosion inhibition of benzoin, benzil, benzoin-(4-phenylthiosemicarbazone) and benzil-(4-phenylthiosemicarbazone) of mild steel in hydrochloric acid, Prot. Met. Phys. Chem. Surf. 51(1) (2015) 143-154, doi: https://doi.org/10.1134/s2070205115010050.

[25] M.A.M.A. Reheim, A.M.E.-S. Tolba, Synthesis and spectral identification of novel stable triazene: As raw material for the synthesis biocompatible surfactants-pyrazole-isoxazole-dihydropyrimidine-tetrahydropyridine derivatives, Int. J. Org. Chem. 06(01) (2016) 44-54, doi: https://doi.org/10.4236/ijoc.2016.61005.

[26] E.-S.A. El-Sharkawy, A.I. Mead, M.A.M. Abdel Reheim, A.M. Tolba, Synthesis and physico-chemical properties of sodium 3-Oxo-2-(3-(4-sulphonatophenyl)triaz-2-enyl)octadecanoate anionic surfactant, J. Surfactants Deterg. 19(3) (2016) 573-582, doi: https://doi.org/10.1007/s11743-016-1810-2.

[27] A. Nagiub, F. Mansfeld, Evaluation of corrosion inhibition of brass in chloride media using EIS and ENA, Corros. Sci. 43(11) (2001) 2147-2171, doi: https://doi.org/10.1016/s0010-938x(01)00006-3.

[28] M. Frisch, G. Trucks, H. Schlegel, G. Scuseria, M. Robb, J. Cheeseman, J. Montgomery Jr, T. Vreven, K. Kudin, J. Burant, Gaussian 03, Revision D01 2004, Gaussian Inc., Wallingford, CT (2004).

[29] M.N. Glukhovtsev, A. Pross, M.P. McGrath, L. Radom, Extension of Gaussian- 2 (G2) theory to bromine- and iodine- containing molecules: Use of effective core potentials, The Journal of Chemical Physics 103(5) (1995) 1878-1885, doi: https://doi.org/10.1063/1.469712.

[30] R.G. Parr, R.A. Donnelly, M. Levy, W.E. Palke, Electronegativity: The density functional viewpoint, The Journal of Chemical Physics 68(8) (1978) 3801-3807, doi: https://doi.org/10.1063/1.436185.

[31] R.G. Parr, R.G. Pearson, Absolute hardness: companion parameter to absolute electronegativity, J. Am. Chem. Soc. 105(26) (1983) 7512-7516, doi: https://doi.org/10.1021/ja00364a005.

[32] R.G. Pearson, Absolute electronegativity and hardness: application to inorganic chemistry, Inorg. Chem. 27(4) (1988) 734-740, doi: https://doi.org/10.1021/ic00277a030.

[33] P. Geerlings, F. De Proft, W. Langenaeker, Conceptual Density Functional Theory, Chem. Rev. 103(5) (2003) 1793-1874, doi: https://doi.org/10.1021/cr990029p.

[34] N.H. Helal, M.M. El-Rabiee, G.M.A. El-Hafez, W.A. Badawy, Environmentally safe corrosion inhibition of Pb in aqueous solutions, J. Alloys Compd. 456(1-2) (2008) 372-378, doi: https://doi.org/10.1016/j.jallcom.2007.02.087.

[35] A.M. Shams El Din, N.J. Paul, Oxide film thickening on some molybdenum-containing stainless steels used in desalination plants, Desalination 69(3) (1988) 251-260, doi: https://doi.org/10.1016/0011-9164(88)80028-6.

[36] H. Al-Deen, Improvement of corrosion resistance of aluminum–bronze alloys in (3.5% NaCL and 2 M HCl) solutions by indium additions, J. Mech. Eng. Res. Dev. 43(2) (2020) 218-225.

[37] M. Mahross, A. Naggar, T.A.S. Elnasr, M. Abdel-Hakim, Effect of rice straw extract as an environmental waste corrosion inhibitor on mild steel in an acidic media, Chem. Adv. Mater. 1(1) (2016) 6-16.

[38] S.A. Ali, A.M. El-Shareef, R.F. Al-Ghamdi, M.T. Saeed, The isoxazolidines: the effects of steric factor and hydrophobic chain length on the corrosion inhibition of mild steel in acidic medium, Corros. Sci. 47(11) (2005) 2659-2678, doi: https://doi.org/10.1016/j.corsci.2004.11.007.

[39] X. Zhang, Y. Zheng, X. Wang, Y. Yan, W. Wu, Corrosion inhibition of N80 steel using novel diquaternary ammonium salts in 15% hydrochloric acid, Ind. Eng. Chem. Res. 53(37) (2014) 14199-14207, doi: https://doi.org/10.1021/ie502405a.

[40] A.S. Fouda, F.E. Heakal, M.S. Radwan, Role of some thiadiazole derivatives as inhibitors for the corrosion of C-steel in 1 M H_2SO_4, J. Appl. Electrochem. 39(3) (2008) 391-402, doi: https://doi.org/10.1007/s10800-008-9684-2.

[41] A.V. Shanbhag, T.V. Venkatesha, B.M. Praveen, S.B. Abd Hamid, Inhibition effects of chloroquinolines on corrosion of mild steel in hydrochloric acid solution, J. Iron. Steel Res. Int. 21(8) (2014) 804-808, doi: https://doi.org/10.1016/s1006-706x(14)60145-x.

[42] T. Peme, L.O. Olasunkanmi, I. Bahadur, A.S. Adekunle, M.M. Kabanda, E.E. Ebenso, Adsorption and corrosion inhibition studies of some selected dyes as corrosion inhibitors for mild steel in acidic medium: Gravimetric, electrochemical, quantum chemical studies and synergistic effect with iodide ions, Molecules 20(9) (2015) 16004-16029, doi: https://doi.org/10.3390/molecules200916004.

[43] M. Yadav, S. Kumar, I. Bahadur, D. Ramjugernath, Corrosion inhibitive effect of synthesized thiourea derivatives on mild steel in a 15% HCl solution, Int. J. ChemTech Res. 9(2014) (2014) 6529-6550.

[44] E. McCafferty, N. Hackerman, Double layer capacitance of iron and corrosion inhibition with polymethylene diamines, J. Electrochem. Soc. 119(2) (1972) 146, doi: https://doi.org/10.1149/1.2404150.

[45] F.M. Mahgoub, B.A. Abdel-Nabey, Y.A. El-Samadisy, Adopting a multipurpose inhibitor to control corrosion of ferrous alloys in cooling water systems, Mater. Chem. Phys. 120(1) (2010) 104-108, doi: https://doi.org/10.1016/j.matchemphys.2009.10.028.

[46] A. Mansri, A. Bendraoua, A. Benmoussa, K. Benhabib, New polyacrylamide [PAM] material formulations for the coagulation/flocculation/decantation process, J. Polym. Environ. 23(4) (2015) 580-587, doi: https://doi.org/10.1007/s10924-015-0734-7.

[47] M. Yadav, R.R. Sinha, T.K. Sarkar, N. Tiwari, Corrosion inhibition effect of pyrazole derivatives on mild steel in hydrochloric acid solution, J. Adhes. Sci. Technol. 29(16) (2015) 1690-1713, doi: https://doi.org/10.1080/01694243.2015.1040979.

[48] N.O. Eddy, S.A. Odoemelam, A.O. Odiongenyi, Inhibitive, adsorption and synergistic studies on ethanol extract ofGnetum Africanaas green corrosion inhibitor for mild steel in H_2SO_4, Green Chem. Lett. Rev. 2(2) (2009) 111-119, doi: https://doi.org/10.1080/17518250903170868.

[49] E.A. Noor, Potential of aqueous extract of Hibiscus sabdariffa leaves for inhibiting the corrosion of aluminum in alkaline solutions, J. Appl. Electrochem. 39(9) (2009) 1465-1475, doi: https://doi.org/10.1007/s10800-009-9826-1.

[50] M. Şahin, S. Bilgiç, H. Yılmaz, The inhibition effects of some cyclic nitrogen compounds on the corrosion of the steel in NaCl mediums, Appl. Surf. Sci. 195(1-4) (2002) 1-7, doi: https://doi.org/10.1016/s0169-4332(01)00783-8.

[51] B.G. Ateya, B.E. El-Anadouli, F.M. El-Nizamy, The effect of thiourea on the corrosion kinetics of mild steel in H_2SO_4, Corros. Sci. 24(6) (1984) 497-507, doi: https://doi.org/10.1016/0010-938x(84)90032-5.

[52] B.M. Mistry, D.H. Kim, S. Jauhari, Analysis of adsorption properties and corrosion inhibition of mild steel in hydrochloric acid solution by synthesized quinoline schiff base derivatives, Trans. Indian Inst. Met. 69(6) (2016) 1297-1309, doi: https://doi.org/10.1007/s12666-015-0690-x.

[53] T. Zhao, G. Mu, The adsorption and corrosion inhibition of anion surfactants on aluminium surface in hydrochloric acid, Corros. Sci. 41(10) (1999) 1937-1944, doi: https://doi.org/10.1016/s0010-938x(99)00029-3.

[54] G.A.H. Gouda, G.A.M. Ali, T.A. Seaf Elnasr, Stability studies of selected metal Ions chelates with 2-(4-amino-1,5-dimethyl-2-phenyl-1,2-dihydro-pyrazol-3-ylideneamino) phenol, Int. J. Nanomater. Chem. 1(2) (2015) 39-44, doi: http://dx.doi.org/10.12785/ijnc/010201.

[55] K.F. Khaled, The inhibition of benzimidazole derivatives on corrosion of iron in 1 M HCl solutions, Electrochim. Acta 48(17) (2003) 2493-2503, doi: https://doi.org/10.1016/s0013-4686(03)00291-3.

[56] A.M. Al-Sabagh, N.M. Nasser, A.A. Farag, M.A. Migahed, A.M.F. Eissa, T. Mahmoud, Structure effect of some amine derivatives on corrosion inhibition efficiency for carbon steel in acidic media using electrochemical and quantum theory methods, Egypt. J. Pet. 22(1) (2013) 101-116, doi: https://doi.org/10.1016/j.ejpe.2012.09.004.

[57] S. Martinez, Inhibitory mechanism of mimosa tannin using molecular modeling and substitutional adsorption isotherms, Mater. Chem. Phys. 77(1) (2003) 97-102, doi: https://doi.org/10.1016/s0254-0584(01)00569-7.

[58] K. Kathirvel, B. Thirumalairaj, M. Jaganathan, Quantum chemical studies on the corrosion inhibition of mild steel by piperidin-4-one derivatives in 1 M H_3PO_4, Open J. Met. 04(04) (2014) 73-85, doi: https://doi.org/10.4236/ojmetal.2014.44009.

[59] O. Olivares, N.V. Likhanova, B. Gómez, J. Navarrete, M.E. Llanos-Serrano, E. Arce, J.M. Hallen, Electrochemical and XPS studies of decylamides of α-amino acids adsorption on carbon steel in acidic environment, Appl. Surf. Sci. 252(8) (2006) 2894-2909, doi: https://doi.org/10.1016/j.apsusc.2005.04.040.

[60] P. Hohenberg, W. Kohn, Inhomogeneous electron gas, Physical Review 136(3B) (1964) B864-B871, doi: https://doi.org/10.1103/physrev.136.b864.

[61] F. Bensajjay, S. Alehyen, M. El Achouri, S. Kertit, Corrosion inhibition of steel by 1- phenyl 5- mercapto 1,2,3,4- tetrazole in acidic environments (0.5 M H_2SO_4 and 1/3 M H_3PO_4), Anti-Corros. Methods Mater. 50(6) (2003) 402-409, doi: https://doi.org/10.1108/00035590310501558.

[62] B.B. Damaskin, O.A. Petrii, V.V. Batrakov, Adsorption of organic compounds on electrodes, Springer US, 1971.

[63] Z. Tao, S. Zhang, W. Li, B. Hou, Corrosion inhibition of mild steel in acidic solution by some oxo-triazole derivatives, Corros. Sci. 51(11) (2009) 2588-2595, doi: https://doi.org/10.1016/j.corsci.2009.06.042.

[64] V.S. Sastri, J.R. Perumareddi, Molecular orbital theoretical studies of some organic corrosion inhibitors, Corrosion 53(8) (1997) 617-622, doi: https://doi.org/10.5006/1.3290294.

[65] I. Lukovits, E. Kálmán, F. Zucchi, Corrosion inhibitors-correlation between electronic structure and efficiency, Corrosion 57(1) (2001) 3-8, doi: https://doi.org/10.5006/1.3290328.